J. Am. Soc. Mass Spectrom. (2017) 28:1623–1637
DOI: 10.1007/s13361-017-1685-0

RESEARCH ARTICLE

An Electrospray Ionization Mass Spectrometry Study on the "In Vacuo" Hetero-Oligomers Formed by the Antimicrobial Peptides, Surfactin and Gramicidin S

Marina Rautenbach,[1,2] N. Maré Vlok,[1,2] Hans A. Eyéghé-Bickong,[1,2] Marthinus J. van der Merwe,[2,3] Marietjie A. Stander[2,3]

[1]BIOPEP® Peptide Group, University of Stellenbosch, Stellenbosch, 7602, Republic of South Africa
[2]Department of Biochemistry, University of Stellenbosch, Stellenbosch, 7602, Republic of South Africa
[3]LCMS Central Analytical Facility, University of Stellenbosch, Stellenbosch, 7602, Republic of South Africa

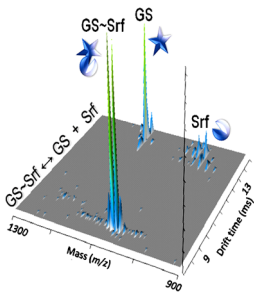

Abstract. It was previously observed that the lipopeptide surfactants in surfactin (Srf) have an antagonistic action towards the highly potent antimicrobial cyclodecapeptide, gramicidin S (GS). This study reports on some of the molecular aspects of the antagonism as investigated through complementary electrospray ionization mass spectrometry techniques. We were able to detect stable 1:1 and 2:1 hetero-oligomers in a mixture of surfactin and gramicidin S. The noncovalent interaction between GS and Srf, with the proposed equilibrium: GS~Srf↔GS+Srf correlated to apparent K_d values of 6–9 μM in gas-phase and 1 μM in aqueous solution. The apparent K_d values decreased with a longer incubation time and indicated a slow oligomerization equilibrium. Furthermore, the low μM K_d^{app} values of GS~Srf↔GS+Srf fell within the biological concentration range and related to the 2- to 3-fold increase in [GS] needed for bacterial growth inhibition in the presence of Srf. Competition studies indicated that neither Na^+ nor Ca^{2+} had a major effect on the stability of preformed heterodimers and that GS in fact out-competed Ca^{2+} and Na^+ from Srf. Traveling wave ion mobility mass spectrometry revealed near symmetrical peaks of the heterodimers correlating to a compact dimer conformation that depend on specific interactions. Collision-induced dissociation studies indicated that the peptide interaction is most probably between one Orn residue in GS and the Asp residue, but not the Glu residue in Srf. We propose that flanking hydrophobic residues in both peptides stabilize the antagonistic and inactive peptide hetero-oligomers and shield the specific polar interactions in an aqueous environment.

Keywords: Surfactin, Gramicidin S, Lipopeptide, Antimicrobial peptide, Antagonism, Molecular interaction, Electrospray ionization mass spectrometry

Received: 7 December 2016/Revised: 8 April 2017/Accepted: 11 April 2017/Published Online: 30 May 2017

Introduction

Rautenbach et al. [1] observed that the anionic lipopeptides in surfactin (Srf) produced by *Bacillus subtilis* protected their producer from the cationic antimicrobial peptide gramicidin S (GS) from *Aneurinibacillus migulanus*. GS is a cyclic decapeptide with a β-sheet structure that contains a repeat pentapeptide moiety with sequence L-Val-L-Orn-L-Leu-D-Phe-L-Pro [2–4] (Figure 1a). The Srf lipopeptide complex contains at least five variant groups of analogous anionic cyclic lipopeptides (Table 1). All these Srf lipopeptides have a β-hydroxy fatty acid (C_{13}, C_{14}, C_{15} or C_{16}) linked via a lactone bond to L-Glu-L-Leu-D-X^1-L-Val-L-Asp-D-Leu-L-X^2, where X^1 can be Leu or Ile and X^2 a Val, Leu, or Ile [5–11] (Figure 1b, Table 1). Noncovalent hetero-oligomers of the lipopeptides in Srf and GS were observed utilizing electrospray ionization mass spectrometry (ESI-MS) [1]. As the participating peptides are amphipathic and membrane active [4, 8, 12, 13], nonspecific complex formation between GS and Srf could involve hydrophobic interactions. More specific electrostatic interactions could take place between the two basic Orn residues in GS and the two acidic residues in Srf, as well as highly specific

Electronic supplementary material The online version of this article (doi:10.1007/s13361-017-1685-0) contains supplementary material, which is available to authorized users.

Correspondence to: Marina Rautenbach; *e-mail:* mra@sun.ac.za

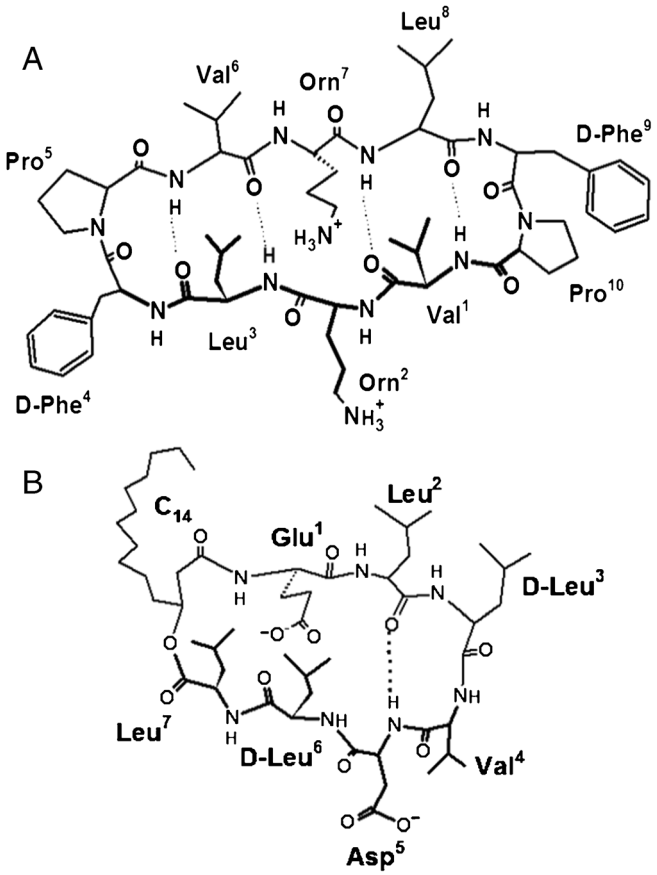

Figure 1. **(a)** Structural model of GS depicting its proposed antiparallel β-sheet conformation [3, 4]. The two Orn and two Phe residues are oriented in one plane, forming the hydrophilic side of the molecule and the hydrophobic side, formed by the two Leu and two Val residues, is directed to the opposite plane of the molecule [12]. **(b)** Structural representation of the S1 model of surfactin [7]. The two acidic amino acid residues Glu^1 and Asp^5 together with Val^4 form the hydrophilic side of the molecule, whereas the four hydrophobic Leu residues are oriented in the other side of the peptide, forming the hydrophobic side. The structures were drawn using ACD/ChemSketch software (ACDLABS 12.0 software)

recognition between the two peptides via dipolar and hydrogen bonding. If neutralizing interaction between GS and Srf results in inactive peptide hetero-oligomers, such interactions between antimicrobial peptides may be a general resistance mechanism allowing peptide-producer microorganisms to co-habituate. Therefore, characterizing the possible noncovalent hetero-oligomer formation and structural influence of Srf on GS would enhance our understanding of this protective and putative resistance mechanism.

ESI-MS is a well-established "soft-ionization" technique for probing noncovalent interactions between biomolecules in gas phase ("in vacuo") [14, 15]. ESI-MS has been used with success in several investigations on noncovalent interaction between peptides [16–19], as well as to determine dissociation constants of interacting biomolecules [20–23]. However, the removal of water and solvent during desolvation of a noncovalent complex during the electrospray process will substantially weaken the hydrophobic forces, and the relative contribution of the hydrophobic and polar interactions will determine the stability of the complex in the gas phase [24–26]. ESI-MS analysis of noncovalent interactions, therefore, limits determination to interacting partners with a strong polar component in their interactions and can also rule out nonspecific hydrophobic aggregation. In the case of Srf and GS, it was important to eliminate the nonspecific contribution of hydrophobic interactions between the two amphipathic peptides, in order to probe the more specific polar interactions.

Alves et al. [18] showed with peptide–DNA complexes that tandem mass spectrometry (MS/MS) can be used to determine the site of ionic interactions. In another MS/MS study on a linear iturin A lipopeptide analogue, it was observed that interaction with a sodium ion stabilized some of the peptide bonds because it chelated to the carbonyl groups in one of the type II β-turns [27]. MS/MS in theory can also be used to probe the interacting residues of two peptides in an oligomer. During MS/MS collision-induced dissociation (CID) of peptides, the majority of fragmentation reactions take place at the peptide (amide) bonds [28, 29]. The sequential product ion spectra are frequently used for de novo sequencing [28, 29]. If a peptide is interacting with another compound via a salt bridge, hydrogen bonds, or other polar/electrostatic bonds, certain peptide bonds and functional groups will be more protected from fragmentation reactions because of group proximity that lead to steric interferences and/or changes in the electronic environment [18, 27]. It is therefore possible that such interactions in the noncovalent hetero-oligomer of GS with Srf can change the ESI-MS fragmentation patterns, and these changes can be used to obtain information regarding sequences, residues, or groups involved in the interaction within GS~Srf hetero-oligomers.

This study describes the first part of an investigation on the molecular interaction between the anionic lipopeptide Srf and the cationic cyclodecapeptide GS. Complementary mass spectrometric data on mixtures of GS with Srf were compared with that of the single peptides in order to probe the conformation, stability, and the possible interaction partners in GS and Srf.

Materials and Methods

Surfactin, gramicidin S, sodium formate, leucine enkephalin acetate salt hydrate (>95%), and poly-DL-alanine were supplied by Sigma-Aldrich (St. Louis, MO, USA). Calcium chloride ($CaCl_2$) was from Associated Chemical Enterprises (Glenvista, South Africa), and sodium chloride (NaCl) from Saarchem (Midrand, South Africa). Acetonitrile (HPLC grade, UV cut-off 190 nm) was supplied by Romil Ltd. (Cambridge, UK). Formic acid (>98%) was purchased from Merck Chemicals (Darmstadt, Germany). A Milli Q water purification system (Merck Millipore, Darmstadt, Germany) was used to filter water from a reverse osmosis plant to prepare analytical grade water.

Table 1. A Summary of the Analysis Data and Proposed Identities of the Different Species in Pure Peptide Samples and an 1:1 Gramicidin S-Surfactin Mixture as Detected with High Resolution ESI-MS, UPLC-MS, and IM-MS

Peptide or heterodimer	Abbr.	Peptide sequence [a] / composition	Theoretical M_r	Ion specie	Theoretical; observed *m/z*	Calculated M_r [b]	UPLC R_t (min) [c]	CCS (Å^2) [d]
Gramicidin S	GS	cyclo[(D-Phe-L-Pro-L-Val-L-Orn-L-Leu)$_2$]	1140.7059	$[M + H]^+$	1141.7137; 1141.7167	1140.7051	-	353±5
				$[M + 2H]^{2+}$	571.3608; 571.3566			334
Surfactin 1	Srf_1	cyclo[($C_{13}H_{24}O_2$)-L-Glu-L-Leu/Ile-D-Leu-L-Val-L-Asp-L-Leu-L-Val]	993.6361	$[M_1 + H]^+$	994.6439; 994.6512	993.6403	10.58	344 (382)
Surfactin 2	Srf_2	cyclo[($C_{14}H_{26}O_2$)- L-Glu-L-Leu/Ile-D-Leu-L-Val-L-Asp-L-Leu-L-Val] cyclo-[($C_{13}H_{24}O_2$)-L-Glu-L-Leu-D-Leu-L-Val-L-Asp-L-Leu-L-Leu/ILe]	1007.6518	$[M_2 + H]^+$	1008.6596; 1008.6644	1007.6552	11.02	348 (386)
Surfactin 3	Srf_3	cyclo[($C_{15}H_{28}O_2$)-L-Glu-L-Leu/Ile-D-Leu-L-Val-L-Asp-L-Leu-L-Val] cyclo[($C_{14}H_{26}O_2$)-L-Glu-L-Leu-D-Leu-L-Val-L-Asp-L-Leu-L-Leu/Ile]	1021.6674	$[M_3 + H]^+$	1022.6752; 1022.6780	1021.6715	11.58;11.68	352 (390)
Surfactin 4	Srf_4	cyclo[($C_{15}H_{28}O_2$)-L-Glu-L-Leu-D-Leu-L-Val-L-Asp-L-Leu-L-Leu/Ile]	1035.6831	$[M_4+H]^+$	1036.6909; 1036.6898	1035.6881	12.07	356 (395)
Surfactin 5	Srf_5	cyclo[($C_{16}H_{30}O_2$)-L-Glu-L-Leu-D-Leu-L-Val-L-Asp-L-Leu-L-Leu/Ile]	1049.6988	$[M_5 + H]^+$	1050.7066; 1050.7050	1049.7032	12.60;12.75	360 (398)
Heterodimer 1	GS~Sr_1	GS, Srf_1	2134.3421	$[M + M_1 + 2H]^{2+}$	1068.1789; 1068.1796	2134.3430	-	519
Heterodimer 2	GS~Sr_2	GS, Srf_2	2148.3577	$[M + M_2 + 2H]^{2+}$	1075.1867; 1075.1984	2148.3638	-	519
Heterodimer 3	GS~Sr_3	GS, Srf_3	2162.3734	$[M + M_3 + 2H]^{2+}$	1082.1945; 1082.1970	2162.3818	-	524
Heterodimer 4	GS~Sr_4	GS, Srf_4	2176.3890	$[M + M_4 + 2H]^{2+}$	1089.2023; 1089.2040	2176.3977	-	527
Heterodimer 5	GS~Sr_5	GS, Srf_5	2190.4047	$[M + M_5 + 2H]^{2+}$	1096.2102; 1096.2190	2190.4102	-	527

[a] GS sequence from [2, 3]; Srf sequences from [5–11]
[b] The experimental M_r for each peptide, variant, or complex was calculated with the MaxEnt 3 algorithm in MassLynx ver. 4.1. Refer to Figures 2 and 9 for representative spectra
[c] Refer to Figure 11 in Supplementary Data
[d] Srf variant CCS values in brackets were corrected with 11.2% according to Goodwin et al. [38]. Refer to methodology and Supplementary Data for details on CCS calculations

Electrospray Ionization Mass Spectrometry

The chemical purity of GS and Srf and the identity of the hetero-oligomers were determined with high resolution ESI-MS utilizing a Waters Synapt G2 Q-TOF mass spectrometer (Milford, MA, USA) fitted with a Z-spray electrospray ionization source (denoted ESI-MS-TOF). GS and Srf were dissolved at 1.00 mM in 50% acetonitrile in water (v/v) and diluted in analytical quality water or 50% acetonitrile in water (v/v) and either analyzed alone or as an equimolar (1:1) mixture of the peptides. Samples pre-incubated at 22 ±2 °C were prepared at least 1 h before analysis. A sample solution (2–5 µL) was introduced into the spectrometer via a Waters Acquity UPLC utilizing direct infusion at a flow rate of 300 µL/min using 0.1% formic acid in 50% acetonitrile/water (v/v/v) as the ESI solvent. The analytes were subjected to a capillary voltage of 2.5 kV, cone voltage (CV) of 25 V, collision energy in trap and transfer collision cell of 4 eV and 0 eV, respectively, a source temperature of 120 °C, desolvation gas (N_2) of 650 L/h, and desolvation temperature of 275 °C. The data were collected in positive mode by scanning through *m/z* = 100–2000 in continuum mode at a rate of 0.2 scans per second. The high resolution mass calibration of the instrument was performed using sodium formate, and in-analysis calibration was performed using leucine enkephalin single point lock spray (*m/z* = 556.2771).

High resolution CID analyses in MS/MS mode on the ESI-MS-TOF instrument were performed by injecting 3 µL of the peptide alone or equimolar peptide mixture (150 µM each in acetonitrile/water) into the mass spectrometer and subjecting the selected precursor ions for decomposition over a collision energy (CE) gradient of 30–80 eV in the trap collision cell with CV at 25 V. Low energy CID was done at 40 eV, with CV set at 30 V. The collision energy in transfer collision cell was set at 0 eV and the collision gas was delivered at 0.5×10^{-3} bar Ar. The isolation *m/z* windows were 1141.7 ± 1, 1022.7 ± 1, and 1182.2 ± 1. Data were collected in the second mass analyzer through *m/z* = 100–2000 in the centroid mode. The rest of the instrument settings were as described above for the MS mode.

Ultraperformance liquid chromatography (UPLC) linked to ESI-MS was performed on ESI-MS-TOF instrument (Waters Synapt G2 linked to the Acquity UPLC system, Dublin, Ireland). Separation of the peptides in the Srf complex (injection of 3 µL of a 1.00 mg/mL sample) via UPLC was done on an Acquity UPLC HSS T3 C_{18} column (1.8 µm particle size, 2.1 × 150 mm; Waters, Dublin, Ireland). Solvents used in the chromatography were: analytical quality water modified with 0.1% formic acid (v/v) (solvent A) and acetonitrile modified with 0.1% formic acid (v/v) (solvent B). The gradient program with the flow rate at 300 µL/min was as follows: 0–0.5 min sample loading at 40% B, 0.5–11 min linear gradient from 40%–95% B, and 11–14 min at 95% B, with re-equilibration from 15–16 min at 40% B. The rest of the instrument settings were as described above for the MS mode, except for the CV, which was set at 15 V.

Ion mobility mass spectrometry (IM-MS) analysis was also utilized for comparative analysis of the peptides and hetero-oligomers. IM-MS on the equimolar mixture (150 µM each) of GS and Srf and the peptides alone was done by enabling the traveling-wave ion mobility cell in the ESI-MS-TOF instrument. The instrument settings were used as above for the MS mode, except for the cone voltage set at 15 V. The traveling-wave IM-MS tuning was as follows: extraction cone at 4 V, helium cell gas flow at 180.00 mL/min, ion mobility buffer gas (N_2) flow at 90 mL/min, trap collision energy at 15 V, a 200 µs trapping release period, mobility trap height at 15 V, mobility extract height at 0 V, wave height ramp (20%) from 8 to 20 V, wave height linear velocity ramp (20%) from 1000 to 650 m/s at 220 m/s. Calibration of traveling wave ion mobility cell's drift time was done by using polyalanine (polyAla) as calibration standard. Refer to the Data Analysis section for details on the collision cross-section (CCS) calculations.

ESI-MS to determine the stability of the peptides and peptide heterodimers and the titration experiments were performed on a Micromass Quattro Triple Quadrupole mass spectrometer fitted with an electrospray ionization source (denoted ESI-MS-TQ). Stock solutions of Srf and GS were dissolved in 50% acetonitrile/water (v/v) and stock solutions of salts ($NaCl_2$ or $CaCl_2$) in 40% acetonitrile/water (v/v). The final solvent concentration before injection was adjusted to 50% acetonitrile/water. Pre-incubated samples were prepared by incubating Srf and the respective salts overnight. GS was added 5 min before analysis to Srf samples. To determine the optimum GS:Srf ratio to study the GS~Srf hetero-oligomers, 125 µM Srf was titrated with 1.25–250 µM GS. To investigate the role of electrostatic interactions in the GS~Srf hetero-oligomers, 90 µM Srf was titrated with 1.11–35.6 mM of either NaCl or $CaCl_2$. In competition assays 90 µM Srf was pre-incubated with 10-fold molar excess NaCl or $CaCl_2$ and then titrated with GS over 1.2–445 µM concentration range.

Samples were injected into the ESI-MS-TQ through a Rheodyne injector valve at 20 µL/analysis with the final carrier solvent concentration 50% acetonitrile/water (v/v). A capillary voltage of 3.5 kV was applied with the ionization source temperature at 80 °C. The cone voltages for the all the analyses were 60 V with the skimmer lens offset at 5 V. Data acquisition was in the positive mode, scanning the mass range through *m/z* = 200–2000 at a scan rate of 100 atomic mass units/s. CID to investigate peptide and heterodimer stability was executed with the CE varied from 5 to 75 eV at a collision cell gas pressure of 2×10^{-3} bar argon. Product ions were detected by scanning the second analyzer from *m/z* = 10 to 100 atomic mass units above the *m/z* value of the precursor/molecular ion. Data were acquired in the multiple channel acquisition mode.

Data Analysis

All graphs were constructed using GraphPad Prism 4.03 (GraphPad Software, San Diego, CA, USA). Sigmoidal and hyperbolic equations were adapted from the GraphPad Prism equation library to fit curves to ESI-MS data.

All mass spectrometric data were analyzed via MassLynx v4.1 SCN 714 (and earlier versions) and Driftscope 2.1 software (Waters, Milford, MA, USA). Continuum mode data were analyzed directly or via the MaxEnt 3 algorithm, while the centroid mode data were analyzed via the TOF transform algorithm. Considering the relationship between analyte ionization and detection in a mass spectrometer, it is possible that the addition of a polar compound such as GS or salts, or decreasing the solvent polarity may influence the ionization characteristics of the other compounds in solution. We therefore calculated the percentage signal contribution of each molecular ion or complex ions of interest to the total peptide signal.

For calibration of the IM-MS drift time, the standard curve of charge corrected CCS (ln Ω′) of polyAla species versus corrected drift time (ln t'_D on X-axis) was constructed according to Ruotolo et al. [30] using the following equations:

$$t'_D = t_0 - \left[\frac{c\sqrt{m/z}}{1000}\right] \tag{1}$$

with $c = 1.4$ (enhanced duty cycle (EDC) delay coefficient) and t_o the observed drift time in milliseconds;

$$\Omega' = \frac{\Omega}{\left[z \times \sqrt{1/\mu}\right]} \tag{2}$$

with z the charge, Ω the CCS for the polyAla specie [31] and $\frac{1}{\mu} = \frac{1}{M} + \frac{1}{m}$ where M is the ion mass of the polyAla specie and m the atomic mass of N_2 (ion mobility drift gas).

The standard curve was fitted to ln Ω′ = Aln t'_D + lnB, where A is the exponential factor used in Equation 3 and B a fitted parameter.

The double correction of t_D was done using the following equation:

$$t''_D = t'^{A}_D \times z \times \sqrt{1/\mu} \tag{3}$$

The CCS values of the individual peptides and complexes were calculated, according to Ruotolo et al. [30], from the polyAla calibration curve of t'_D versus CCS (or Ω) values from literature [31]. Refer to Supplementary Data for detail on the CCS result for polyAla calibration (Supplementary Figure 12A).

The collision energy (CE) to fragment or dissociate 50% of the molecular ion specie, which is an approximation of 50% of E_{LAB} or laboratory frame energy to fragment/dissociate molecular ions [32, 33], is denoted as CE_{50} and was calculated by fitting a Boltzman sigmoidal curve with the equation (Equation 4):

$$Y = Y_{\min} + {}^{(Y_{\max}-Y_{\min})}\Big/_{(1+e)}(CE_{50}-\times)\Big/slope \tag{4}$$

where Y is the % loss of ion abundance of each of the different heterodimer species, Srf variants and GS that is recorded for each CE, Y_{min} the minimum % loss in ion abundance approximating zero (bottom of sigmoid), Y_{max} the maximum % loss in abundance approximating 100% (top of sigmoid), and CE_{50} the CE at 50% response, with x the set CE from 10 to 75 eV.

Center of mass collision energy or E_{CM} was calculated from the following equation:

$$E_{CM} = E_{LAB} \times m_{Ar}/(m_{Ar} + M) \tag{5}$$

where E_{LAB} is taken as the set CE, m is the atomic mass of the collision gas argon, and M the molar mass of the peptide ion or heterodimer ion [32, 33].

The GS where half maximal GS~Srf ion abundance is reached, denoted as C_{50}, was calculated from the ESI-MS titration data (refer to Figures 5 and 6 under Results and Discussion) by fitting a sigmoidal curve with variable slope using a four parameter logistic equation:

$$Y = Y_{\min} + {}^{(Y_{\max}-Y_{\min})}\Big/_{(1+10)}(\log C_{50}-\times) \times slope \tag{6}$$

where Y is the % ion abundance of each of the different heterodimer species (or Srf variants) that is recorded for each GS concentration, Y_{min} the minimum % ion abundance approximating zero (fitted bottom of sigmoid), Y_{max} the maximum ion abundance approximating saturation (fitted top of sigmoid), and x is the logarithm of GS concentration.

The apparent dissociation constant ($K_d{}^{app}$) for GS~Srf↔GS + Srf in the gas phase was calculated from the ESI-MS-TOF spectra with CV at 25 V (example of spectrum shown in Figure 2) using an equation adapted from [34]:

$$K_d^{app} = \left(R \times I_{Srf}\Big/I_{GS\sim Srf}\right)\Big/\left(1+R \times I_{Srf}\Big/I_{GS\sim Srf}\right) \tag{7}$$

where I is the signal intensity and R is the ratio of the response factors (f) of the molecular ions $[GS \sim Srf + 2H]^{2+}$ and $[Srf + H]^+$ [34, 35]. We calculated a relative f for Srf ($f_{Srf} = (I_{Srf}/I_{GS}) \times 1.00$), using the signal intensities at standard concentrations (150 and 200 μM) and different injection volumes (3, 4, and 5 μL) as 1.0 ± 0.1 (n = 6). Total signal intensity of each ion was derived using the MaxEnt 3 algorithm considering m/z from 800 to 3000. As it was not possible to obtain a true f for $[GS \sim Srf + 2H]^{2+}$, we had to make an assumption that $R = 1.0$. C_0 was taken as [Srf] + [GS~Srf] = [GS]+[GS~Srf]. The term $I_{GS\sim Srf}$ denotes the sum of the signals from heterodimeric complexes GS ~ $Srf_{1\text{-}5}$ and I_{Srf} the sum of the signals of Srf_1, Srf_2, Srf_3, Srf_4, and Srf_5 (refer to Table 1 for structures).

Circular dichroism data from a previous study on GS and Srf interaction [1] was used to calculate the $K_d{}^{app}$ for solution-phase interaction. The average molar ellipticity at 206 ± 3 nm from the monomer-heterodimer model for GS ~ Srf ↔ GS + Srf, was used in the following equation from [36]:

$$K_d^{app} = {}^{[GS]\times[Srf]}\Big/_{[GS\sim Srf]} = 2P_t \times (1-f_t)^2\Big/f_t \tag{8}$$

where P_t is the total peptide concentration and $f_t = (\theta_{observed} - \theta_{oligomer})/(\theta_{GS\ in\ TFE} - \theta_{oligomer})$; $\theta_{oligomer}$ was taken as 20.7 ×

10^3 deg.cm^2·dmol^{-1}, as determined from a pre-incubated sample of GS and Srf.

Results and Discussion

Detection of the ESI-MS Stable Srf-GS Complexes

When an equimolar mixture of GS and Srf in 50% acetonitrile was subjected to ESI-MS-TOF analysis, a considerably lower Srf signal was detected, compared with the intense doubly charged specie of GS at *m/z* 571.36 (Figure 2). This difference was expected as the five lipopeptide variant groups in the Srf complex (refer to Table 1 for structures) are neutral at acidic pH and negative at neutral pH. The Srf signals are lower because these lipopeptides Srf will only be protonated (charged) on one of the amides in the MS source as the ESI-MS was performed in the positive mode. However, the combined signals and response of the singly charged Srf ions were highly comparable to the singly charged GS ion at 1141.71 (Figure 2), and we therefore focused these ion signals in the analysis and calculations. Refer to the Supplementary Data for details on the spectra of the individual peptides (Supplementary Figure 9).

In addition to the individual peptide species, the mixture of GS and Srf contained a range of molecular species corresponding to the *m/z* ratios of doubly charged peptide heterodimers (GS~Srf) (C_1–C_5 in Figure 2, Table 1). Low CE CID of GS~Srf_3 (*m/z* 1082.18) showed that this molecular ion complex is composed of GS and the Srf_3 variants with M_r = 1022.65 (Supplementary Data, Supplementary Figure 10). The identified components in the GS~Srf_3 and other GS~Srf heterodimers are listed in Table 1.

In addition to the 1:1 hetero-oligomers, low abundance 1:2 (GS~2Srf) and 2:1 (2GS~Srf) oligomers were also detected in some samples (insert in top spectrum of Figure 2). No triply charged or quadruply charged species corresponding to hetero-oligomers were detected in our analysis over the *m/z* = 200–2000. In subsequent analyses over a broader *m/z* range, we also did not detect doubly changed hetero-oligomer ions containing three Srf or three GS molecules (results not shown). As Srf_5, GS~Srf_5, and the heterotrimeric complexes had low abundance in our samples subjected to ESI-MS analysis, we focused the rest of this study on $Srf_{1\text{-}4}$ variants and GS~$Srf_{1\text{-}4}$ heterodimers (Figure 2, Table 1).

The complexes that formed were further assessed with IM-MS to determine if the GS~Srf heterodimers had multiple conformers, which would indicate a more random or less specific peptide association (Figure 3). We examined the pure peptides and found that both GS and the Srf variants had a drift time (or arrival time) around 13 ms (compare Figure 3a with c). Three drift peaks of the $[GS + H]^+$ molecular specie indicated at least three GS conformers and corresponded to CCS of 353 ± 5 Å^2 (Figure 3c), which is about 35% larger than the CSS for GS in He observed by Ruotolo et al. [37]. A change in the GS profile was observed for the peptide mixture, which yielded only one major peak at CCS of 353 Å^2 for GS (compare Figure 3c with d). It has previously been shown that GS has different conformers [3, 4, 37] and this result is a strong indication that certain conformers of GS (CCS 348 Å^2 and 358 Å^2) preferentially bound to Srf.

Similarly to Srf variant retention on C_{18}-UPLC matrix, the ion drift time of the singly charged $Srf_{1\text{-}4}$ variants in the pure peptide complex increased linearly with M_r and there is a direct linear correlation between drift time (t_D') and UPLC R_t (Supplementary Figure 12C and D in Supplementary Data). This indicated that the larger Srf variants with longer fatty acyl chains and Leu/Ile instead of Val in their peptide sequence moved slower through the ion mobility cell because of their larger CCS (refer to Table 1 for more detail). Furthermore, they were retained longer on the C_{18} matrix in the same order because their increase in size correlated directly with an increase in hydrophobicity that translated from the longer fatty acyl chain and Leu/Ile instead of Val (Supplementary Data, Supplementary Figures 11 and 12). Drift peaks of the five Srf variants clustered with derived CCS values between 344 and 360 Å^2 (Figure 3a, Table 1). Goodwin et al. [38] found that CCS calibration with linear peptides such as those in the polyAla preparation led to an underestimation of CCS values of cyclic peptides. We calculated that the derived CCS values for the Srf variants may be underestimated by about 11% (refer to Supplementary Data, Supplementary Figure 12B). Regardless, there is approximately a 4 Å^2 incremental increase from Srf_1 to the largest group Srf_5, indicating an identical/incremental change in structure, possibly the elongation/methylation of the fatty acyl chain. The profile of the Srf variants changed in the equimolar peptide mixture and we observed two main peaks (compare Figure 3a with b). This can be due to the loss of some Srf variants because they preferentially interacted with GS and were transferred into a GS~Srf oligomer.

Only heterodimeric complexes of GS~Srf were observed, probably because of the lower sensitivity in the IM-mode and/or because the lower abundance larger oligomers did not survive the ion mobility cell (Figure 3e–h). The doubly charged ions of GS~Srf_1 and GS~Srf_2 heterodimers both had a drift time corresponding to a CCS of 519 Å^2, whereas slightly larger CSS values of 524 Å^2 and 527 Å^2 were observed for the more hydrophobic GS~Srf_3 and GS~Srf_4 heterodimers, respectively (Table 1, Figure 3). These clustered CCS values and narrow, nearly symmetrical IM-MS peaks indicate that the heterodimers have similar conformations and that the two peptides have a compact structure due to specific interactions. The contribution of each of the Srf variants to the complex was calculated from the IM-MS profiles as: GS~Srf_1 = 3%, GS~Srf_2 =11%, GS~Srf_3 = 43%, and GS~Srf_4 = 43%. These IM-MS detected abundances indicated that the surviving heterodimers were not directly related to the Srf variant abundance but rather to the differences in hydrophobicity of the interacting Srf variants, as determined by C_{18}-UPLC-MS, which will naturally reflect in the heterodimers (refer to Supplementary Data, Supplementary Figures 11 and 12).

Stability of the Peptides and GS~Srf Hetero-Oligomers

CID experiments were performed with the ESI-MS-TQ to evaluate the relative gas-phase stability of the peptides and

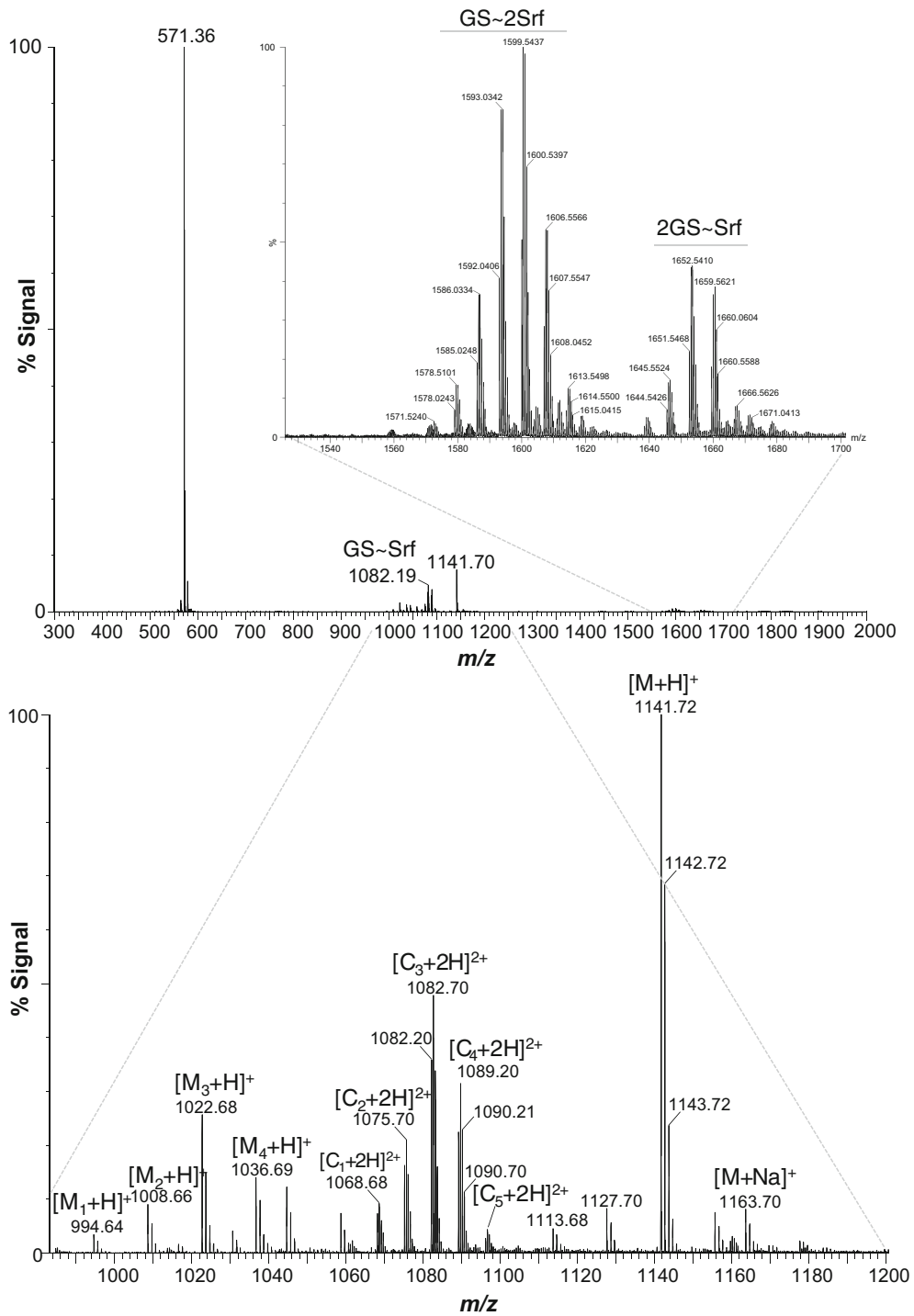

Figure 2. A representative ESI-MS-TOF ion spectrum of an equimolar Srf-GS mixture. The top spectrum shows the signal comparison of the intense doubly charged specie of GS at *m/z* 571.36, with the singly charged GS specie at *m/z* 1141.7, as well the oligomeric species (GS~Srf). The extracted heterotrimeric specie spectrum is shown in the insert of the top spectrum. The extracted bottom spectrum shows singly charged GS (denoted M) and four different singly charged Srf variants (M_1–M_4). The five doubly charged 1:1 GS~Srf heterodimers (denoted C_1–C_5) are also indicated

their heterodimeric complexes (Figure 4). CID induces a unimolecular decay of selected ions with sufficient internal energy upon collision with a neutral gas [39] and CID-derived binding energy of noncovalent complexes reflect the order of solution phase binding energies [21, 22]. The CID results indicated that all the Srf variants required a similar CE_{50} with an average of 34.0 ± 0.4 eV. The apparent stability of GS was significantly higher at CE_{50} = 42.3 ± 2 eV than the different Srf variants. If only the CE is considered, the various GS~Srf heterodimers showed similar stabilities during CID,

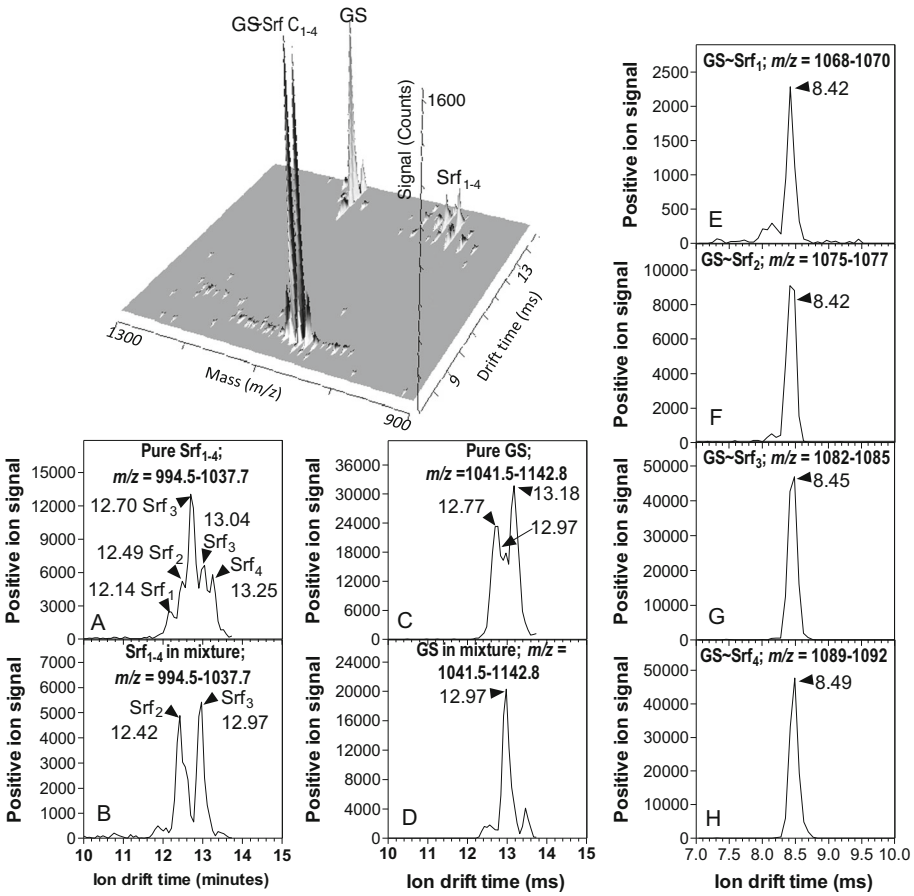

Figure 3. A representative 3D IM-MS graph of the equimolar Srf:GS mixture (top graph) and IM-MS of pure Srf **(a)** and GS **(c)** and their extracted profiles **(b)** and **(d)**, respectively, in an equimolar Srf:GS mixture. Both the singly charged ions of Srf_{1-4} variants of Srf alone **(a)**, or in the mixture **(b)**, and the GS ion, alone **(c)**, or in the mixture **(d)** showed a drift time around 13 ms. The extracted ion mobility profiles of the four doubly charged GS~Srf heterodimeric complexes ($GS{\sim}Srf_{1-4}$) in the mixture were detected at 8.42 ms for $GS{\sim}Srf_1$ **(e)** and $GS{\sim}Srf_2$ **(f)**, 8.45 ms for $GS{\sim}Srf_3$ **(g)** and 8.49 ms for $GS{\sim}Srf_4$ **(h)**. For the extracted ion profiles the major isotopic peaks for each peptide or complex were considered

but these noncovalent heterodimers were more unstable than the individual peptides with an average CE_{50} of 18.9 ± 0.1 eV (Figure 4a).

Slightly different CCS values were found for the different Srf variants, as deduced from their traveling wave IM behavior (Figure 3, Table 1). Differences in CCS, molecular volume, area, and mass of the peptides and complexes, as well as differences in charge complicate the interpretation of the CE_{50} results in terms of comparative stability. As an increase of size leads to an increase in CCS of a molecule and the larger CCS of complexes will statistically collide with more target gas atoms than the individual peptides, this may lead to increased fragmentation. On the other hand, smaller molecules have higher kinetic energy that can also translate into increased fragmentation reactions. The center-of-mass CE (E_{CM}) takes the size of the molecule into account and was calculated to directly compare the stability of the different peptides and heterodimeric complexes [32, 33]. The expected exponential decrease in detection of intact molecular ions was found when E_{CM} was plotted against the ion abundance. The trends of the semi-log plots revealed a distinct difference in stability (Figure 4b, c). GS had a similar stability to the smaller, less hydrophobic Srf_1 and Srf_2 variants, which in turn were more stable than the more hydrophobic variants in Srf_3 and Srf_4 groups (compare slopes in Figure 4b). In the case of these peptides, the enhancing effect of higher kinetic energy of the smaller peptides on fragmentation reactions was probably outweighed by the differences in CCS. The stability difference can possibly be attributed to a more rapid decomposition of the slightly larger Srf_3 and Srf_4 variants (CCS 352 $Å^2$ and 356 $Å^2$, respectively), versus the smaller Srf_1 and Srf_2 variants (CCS 344 $Å^2$ and 348 $Å^2$, respectively) and cationic, more fragmentation-resistant peptide chain of GS [39] (refer to Table 1 for peptide structures).

The GS~Srf heterodimers containing the smaller Srf_1 and Srf_2 variants showed a similar trend with $GS{\sim}Srf_1$ being significantly more stable than $GS{\sim}Srf_2$ (compare slopes in Figure 4c). $GS{\sim}Srf_3$ and $GS{\sim}Srf_4$ were observed to be less stable than $GS{\sim}Srf_1$ and $GS{\sim}Srf_2$ (compare slopes in Figure 4c, refer to Table 1 for structures). However, some weak Van der Waals forces (hydrophobic interactions) may survive under certain ESI-MS conditions as we observed higher survival/abundance of $GS{\sim}Srf_3$ and $GS{\sim}Srf_4$ during normal mode

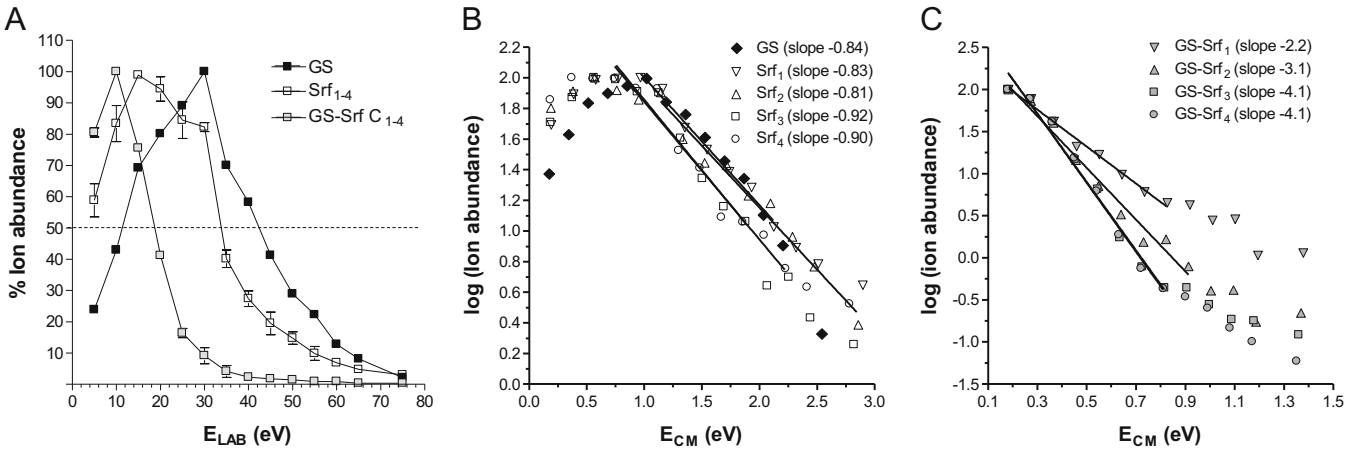

Figure 4. ESI-MS-TQ stability of GS, Srf, and GS~Srf heterodimers. **(a)** CID of GS, Srf_{1-4} (average of Srf_{1-4} ± standard error of the mean, SEM), and GS~Srf heterodimers (average of GS~Srf_{1-4} ± SEM); CE was varied from 5 to 75 eV with cone voltage set to 60 V. The dotted line shows the CE_{50} cutoff. Normalization to 100% was done using the highest signal for each molecular ion. **(b)** Semi-log linear relationship (solid lines) of E_{CM} (calculated with Equation 5 [32, 33]) with the peptides alone, and **(c)** with the different GS~Srf heterodimers. Linear regression analyses were done on the data points where at least seven consecutive points showed a linear response with the steepest slope. All the linear fits gave $R^2 > 0.95$

ESI-MS and IM-MS. This stability difference probably relates to a total loss in residual hydrophobic forces for the heterodimers containing more hydrophobic Srf_3 and Srf_4 variants during the high energy CID exposure in the gas phase [19, 24, 25]. Furthermore, the difference between IM-MS and CID stability is probably due to the lower energy experienced in the ion mobility cell versus that in the collision mode, which not only constitutes a higher CE but also a higher concentration of collision gas (argon).

Interaction Parameters of the GS~Srf Hetero-Oligomers

Antimicrobial peptides are dependent on both electrostatic and hydrophobic interactions with their target membranes. Similar interactions are possible between the two peptides in this study to form the hypothesized complexes or hetero-oligomers. Srf, an anionic lipopeptide containing a fatty acyl group, is considerably more hydrophobic than the cationic amphipathic GS. Therefore the two peptides can interact via hydrophobic interactions, which are generally more non-specific. More specific ionic interactions can take place between the two cationic Orn residues of GS and the anionic Asp and Glu residues in Srf. As there are also a number of functional groups in these peptides, polar or electrostatic interactions, such as dipole interactions and hydrogen bonds in more hydrophobic environments, such as membranes, are also highly probable.

It is well-known that hydrophobic interactions are highly dependent on the polarity of the solvent and a strong driving force in water for interaction between hydrophobic and/or amphipathic molecules. Conversely, the ionic/polar/electrostatic interactions are weaker in an aqueous environment, but will naturally increase in a nonpolar solvent or when a noncovalent complex is transferred from an aqueous solvent into gas phase, such as during ESI-MS [26]. We therefore focused on the polar/electrostatic interactions in the GS~Srf hetero-oligomers. These polar forces are the major contributors in "in vacuo" interactions between compounds in the ESI-MS in which the hydrophobic force and concomitant Van der Waals interactions are highly weakened [24–26].

When the individual Srf variants and GS~Srf heterodimers were followed with ESI-MS-TQ over a GS concentration range, a classic sigmoidal concentration-dependent curve was observed for both the free Srf variants and the heterodimeric complexes (Figure 5b). Without making any assumptions, we used Equation 6 to calculate a C_{50} or [GS] leading to a 50% change in a specific Srf or GS~Srf ion signal and found an average C_{50} of 9.9 ± 0.4 μM with saturation and loss of Srf signal from 32 to 64 μM GS. As the Srf concentration was 125 μM and Srf signals decreased to <10%, this is a strong indication that we did not detect neutral hetero-oligomers and/or larger oligomers.

Utilizing ESI-MS we determined an "in vacuo" or apparent dissociation constant (K_d^{app}) for the equilibrium GS ~ Srf ↔ GS + Srf by incubating equimolar peptide mixtures. K_d^{app} values were calculated, using Equation 7 [34], as 6.1 ± 1.1 μM (n = 8) for the pre-incubated peptide mixtures and as 9.2 ± 1.2 μM (n = 8) for the directly analyzed peptide mixtures. These K_d^{app} values were significantly different ($P < 0.0001$) and the decrease indicated a slow equilibrium. For a slow assembling process, the initial hydrophobic interactions between Srf and GS can lead to "seeding" oligomers, which subsequently rearranges over time into more stable hetero-oligomers that are not solely dependent on hydrophobic interactions. We then used circular dichroism data from a previous study on GS and Srf interaction [1] and calculated a solution phase K_d^{app} of 1.2 ± 0.2 μM for a pre-incubated sample using Equation 8 [36]. As our focus is on the in vacuo interaction, a more detailed study on solution-phase molecular interaction between Srf and GS will be reported elsewhere. The observed

in vacuo K_d^{app} for the pre-incubated sample was thus about 5-fold higher than the K_d^{app} calculated for interaction in an aqueous solution. Because the hetero-oligomers are exposed to the harsh conditions during the ESI-MS analysis (high source and desolvation temperatures, low pH, organic solvents, and high voltages), there is most probably a loss of weaker seeding oligomers in the gas phase leading to a higher K_d^{app} for GS ~ Srf ↔ GS + Srf than in aqueous solution. This higher in vacuo K_d^{app} could therefore be due to the loss of the hydrophobic interactions, as well as an underestimation of the K_d^{app} due to the approximated R used in Equation 7. It must also be considered that the ESI-MS analysis does not allow the observation of neutral oligomeric species and higher order oligomers, while the probability of neutral and/or larger oligomers was indicated by our titration studies (Figure 5, refer to discussion above).

Binding Interactions Between GS and Srf

Ionic interactions between GS and Srf are highly probable as GS has a 2+ charge and Srf a 2− charge at neutral pH. Danders et al. [40] and Nagamurthi and Raubhav [41] showed that more than 98% of GS activity is lost when the two Orn residues are blocked with different groups. Acetylated GS, in which both the amino groups of the Orn residues were acetylated, did not show any ESI-MS stable hetero-oligomers with Srf (Supplementary Figure 13, Supplementary Data). This indicated that at least one of the two Orn δ-amino groups of GS is necessary for interaction with Srf or to form stable ESI-MS detectable oligomers.

It was previously shown that the carboxyl groups of L-Glu[1] and L-Asp[5] residues of Srf chelates both mono- and divalent cations, resulting in either partial or complete neutralization of the acidic residues [13, 42–46]. Since metal ion binding neutralizes the acidic residues, it offers a tool to investigate the possibility of an ionic interaction with these residues through competition studies. Addition of NaCl or $CaCl_2$ to the peptide mixtures did not affect the signals of preformed ESI-MS-TQ stable complexes up to 35.6 mM NaCl and $CaCl_2$ (400-fold molar excess) (Supplementary Figure 14 in Supplementary Data). The ESI-MS signal of all the heterodimeric GS~Srf complexes remained reasonably constant over both salt concentration ranges (Supplementary Figure 14 in Supplementary Data). Similarly, GS signal intensity was generally unaffected by increasing salt concentrations. Signal intensity of Srf showed some fluctuation over the NaCl concentration range with a decrease in intensity at 35.6 mM salt, which is probably the result of signal suppression by Cl^- ions and Srf~Na complexation leading to the increase in the detection of the sodiated Srf (Supplementary Figure 14 in Supplementary Data). However, less than 1% sodiated or calciated GS~Srf complexes were detected under these analyses conditions, indicating that these complexes are either unstable or not formed. Addition of Na^+ or Ca^{2+} to preformed GS~Srf hetero-oligomers does not displace GS from Srf, which indicates that the interaction is more complex than just pure ionic interactions between two oppositely charged peptides. However, this result does not rule out the possibility of ionic interaction as one of the interacting forces because an Asp~Orn and/or Glu~Orn salt-bridge could be buried and shielded within the preformed hetero-oligomers.

This aspect was further investigated by pre-incubation of Srf with salts and then titration with the GS. As there is always some environmental Na^+ in solvents, for example sodium leaching from soda glass, the sodium adducts of Srf variants, in particular for the Srf_3 variants, are generally observed in ESI-MS spectra. We found that the Srf_3~Na complex (and other sodiated complexes) decreased in the same manner as the free Srf_3 with the increase in GS and GS~Srf complexes (Figure 5a), indicating that GS out-competes Na^+ from Srf.

As it is known that Srf forms ionic complexes via L-Glu[1] and L-Asp[5] residues with Ca^{2+} [13, 42–46], the effect of GS on Srf~Ca complexes was investigated by the titration of Srf pre-

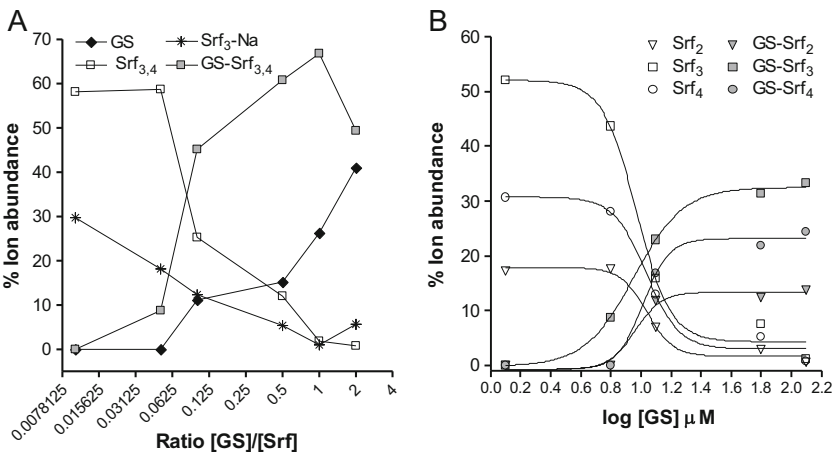

Figure 5. Influence of GS concentration on the formation and detection of GS~Srf heterodimers, as well as detection of Srf and GS ($[M + H]^+$) using the ESI-MS-TQ. Srf at 125 µM was titrated with GS. **(a)** The results of a representative titration experiment with total abundance of $Srf_{3,4}$ variants and GS~$Srf_{3,4}$. **(b)** Sigmoidal response of each of the Srf_{2-4} variants and GS~Srf_{2-4} heterodimers to calculate the C_{50} values for GS binding to Srf. Percentage ion abundance was calculated in terms of the total molecular ion intensity of the monitored ions in each sample

incubated with $CaCl_2$ with GS. In the samples without GS, we observed calcium–Srf complexes consistent with other reports [13, 42, 44]. These monomeric and dimeric complexes all consisted of Srf~Ca in an 1:1 ratio. When the calcium-incubated Srf was then titrated with GS, the observed ESI-MS spectral changes indicated that GS~Srf complex formation takes place in favor of Srf~Ca complex (Figure 6).

All the Srf~Ca complexes decreased over the whole GS concentration range (Figure 6b), similar to that of the free Srf species with Srf_3 and Srf_4 showing the highest free peptide signal at low GS (Figure 6a). In the reagent mixture containing $CaCl_2$, at the lowest concentration of GS, the GS~Srf_2 signal was the highest, but decreased with the GS concentration increase, whereas GS~Srf_1 remained relatively constant. However, GS~Srf_3 and GS~Srf_4 concomitantly increased with the Srf and Srf~Ca decrease, indicating a dynamic exchange/equilibrium from GS~Srf_2 in favor of GS~Srf_3 and GS~Srf_4 at higher GS concentrations (Figure 6c). GS~Srf_3 and GS~Srf_4 each increased up to 45 µM GS (GS:2Srf ratio), after which the signal remained relatively constant (Figure 6c). It is interesting to note that the free GS signal only started to substantially increase at >40 µM. The total GS~Srf and GS~2Srf oligomer signals increased over the entire concentration range, with a concomitant decrease in Srf, Srf~Ca, and 2Srf~2Ca ion signals (Figure 6d). The K_d^{app} for GS ~ Srf ↔ GS + Srf in the presence of Ca^{2+}, calculated from Equation 7, was 17 ± 4 µM. This K_d^{app} is nearly 2-fold higher than the K_d^{app} for the directly analyzed mixtures without Ca^{2+}. This result indicates that GS still binds to Srf in the presence of Ca^{2+}, but that GS may have to compete with Ca^{2+} for binding to Srf or that the specific Ca^{2+}-induced Srf conformation [43, 47] has a weaker affinity for GS.

The hetero-trimer ion signals for GS bound to two Srf species were again detected and increased over the GS concentration range, but were much less pronounced than the 1:1 heterodimers (Figure 6d). We also observed that GS addition interferes with multimeric Ca~nSrf complexes, which may indicate that GS out-competes calcium from the dimeric complexes to form GS~2Srf (Figure 6d). Alternatively, as the Srf concentrations were more than 10-fold the critical micellular concentration (CMC) of 7.5 µM [46], the interaction of GS may be with the micellular Srf [43, 47], of which the hydrophobic interactions are disrupted during the ESI-MS desolvation process. However, the significance of cyclic peptide β-turns in cation chelating has previously been

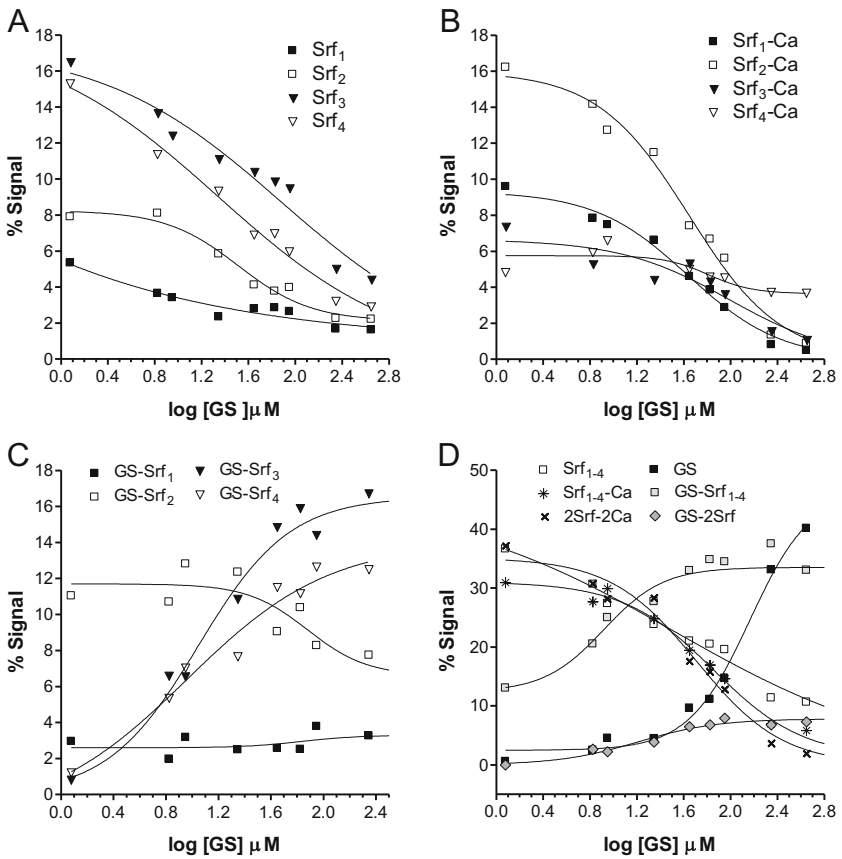

Figure 6. The influence pre-incubation of 90 µM Srf with 10-fold excess $CaCl_2$ on the formation/detection of GS~Srf hetero-oligomers when titrated with GS as analyzed with ESI-MS-TQ. **(a)** %Signal of Srf variants 1–4 over the GS concentration range; **(b)** % signal of Srf variants 1–4 oligomerized with Ca^{2+} over the GS concentration range; **(c)** %Signal of GS oligomerized to Srf variants 1–4 over the GS concentration range; **(d)** averaged %signal of the different Srf, Srf~Ca, 2Srf~2Ca, GS~Srf, GS~2Srf, and GS molecular species over the GS concentration range. Data are the average of two titration experiments (only $[M + H]^+$ depicted for GS). Normalization of signal data was done using sum of the ion signals of the participating ion species as 100%

demonstrated for the analogous lipopeptide, iturin A [27, 48]; therefore, it is also possible for a cationic δ-amino group of Orn in GS to interact via ion-dipole interactions with the carbonyl groups in a β-turn in Srf [8, 44]. Regardless of the oligomeric state of Srf, these results show that GS competes with Ca^{2+} for binding to the anionic Srf or that GS changes Srf's affinity for Ca^{2+} by its initial interaction and subsequent binding. These observations also support the role of hydrophobic interactions in that the less hydrophobic Srf_1 and Srf_2 species seem to favor Ca^{2+} interaction, whereas the more hydrophobic Srf_3 and Srf_4 species favor GS interaction.

CID of a GS~Srf Heterodimer

To further explore noncovalent interaction, the oligomerization between GS and surfactin were investigated utilizing CID. In an oligomer, certain peptide bonds will be protected from fragmentation when they are either hidden or partaking in polar or hydrogen bonds. A change in peptide conformation in an oligomer could, on the other hand, expose certain bonds to fragmentation reactions. However, it is highly possible that during CID process all noncovalent interactions within an oligomer will be broken prior to the covalent fragmentation. If this is the case, identical fragmentation patterns will be observed between the free peptides and those liberated from the oligomer, albeit at lower intensity. If there is a change in product ion pattern, this could indicate strong interactions in hetero-oligomers leading to altered fragmentation of peptide bound in the oligomer. This altered fragmentation was indeed observed in this study, which indicated that some of the fragmentation reactions took place within the GS~Srf heterodimer. These changes were used to identify residues and sequences that partake in the polar interactions within a GS~Srf heterodimer.

One of the prerequisites in the fragmentation of cyclic peptides is the controlled opening of the backbone ring. For GS, the ring opening mostly occurs at the N-terminal side of one of the Pro residues [49, 50] as a consequence of the preferential fragmentation of the N-terminal peptide bond of Pro [51, 52]. A second ring opening is between the Orn-Leu residues [49, 50] and this frequently leads to the so-called "ornithine effect" [53, 54]. During this, a fragmentation reaction at the C-terminal of an Orn residue leads to cyclisation in which the Orn side chain participates [53, 54]. The CID on the singly charged GS (*m/z* = 1141.7137) yielded all the major fragment ions from the b-series, except b_6 (PVOLFPV) arising from the ring-opening of GS at one of the Pro-Val moieties, correlating with previous research (Figure 7a) [49, 50]. The absence of this b_6-ion is expected as the C-terminal bond of a Pro-residue is more stable than the N-terminal bond, although a low abundance b_3 ion (LFP), probably derived from the Orn-Leu ring opening, was observed [51, 52]. Internal fragments or b-ions from a Phe-Pro ring-opening were also abundant in the CID spectrum of GS (Figure 7a). The b_2-ion and its a_2-ion, corresponding to the Pro-Val sequence, were the most abundant product ions (25%–30% abundance) observed for the free GS, probably because of the inherent stability of the C-terminal peptide bond with Pro [51, 52] (Figure 7a). Most of the GS product ions generated from GS~Srf_3 were similar to that of free GS; however, there were a number of major differences in the product ion pattern (Figure 7a). The b_5 ion (PVOLF or LFPVO), one of the most abundant product ions in the free GS spectrum, was not observed upon CID of the heterodimer ion (*m/z* 1082.1945), whereas the dehydrated b_5 ion abundance decreased significantly (Figures 7 and 8). In our initial CID analyses, we did observe the b_5 ion in the CID spectrum of GS from GS~Srf_3, but we found this was due to persistent GS contamination in the instrument from previous analyses (results not shown). No FPV and LFP product ions were observed, whereas the b_2 ion, PV, almost doubled in abundance (Figure 7a). The increased b_2 abundance could also indicate

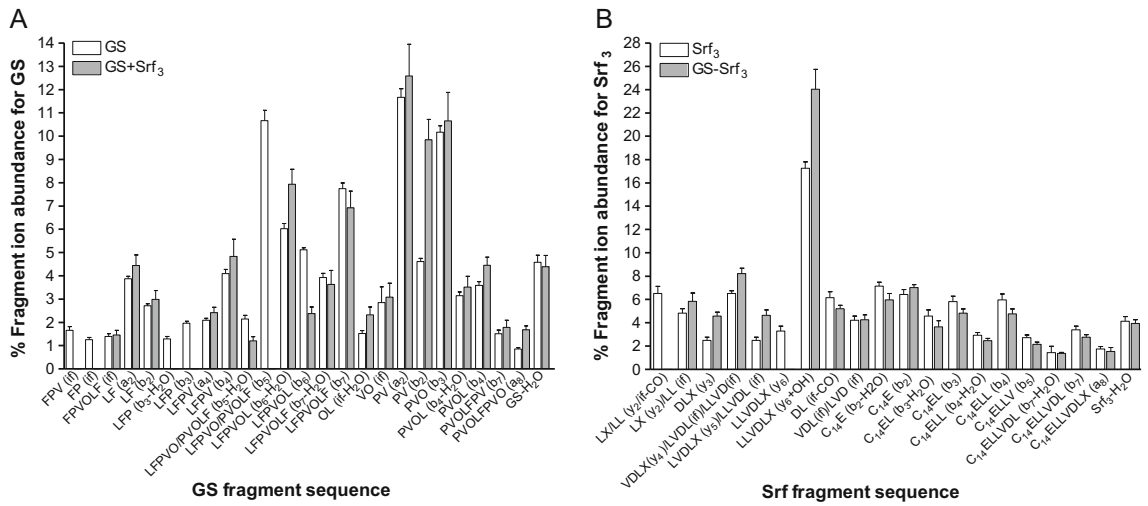

Figure 7. Comparison of CID generated product ions of GS and Srf alone and from the GS~Srf_3 heterodimer. **(a)** Comparative bar graph of the GS product ions, and **(b)** Srf product ions with X being either Ile or Leu. Data are the average ± standard deviation of nine and five CID spectra for the free peptides and heterodimer, respectively. Representative CID spectra are supplied in Supplementary Figure 15 and for details on product ions refer to Supplementary Table 2 (Supplementary Data)

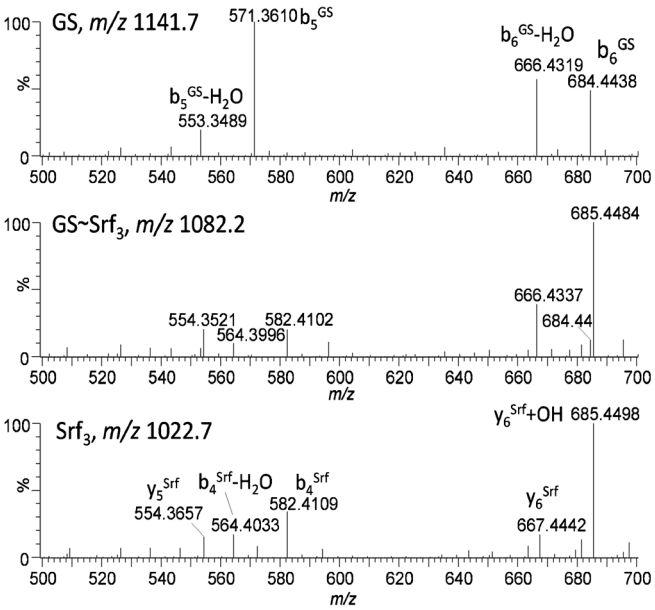

Figure 8. Representative CID spectra over *m/z* 500–700 for comparison of CID product ions of GS and Srf alone with that of GS~Srf_3 heterodimer. CID analyses were performed over a CE gradient from 30 to 80 eV at a CV of 25 V. For more details on the product ions, refer to Supplementary Table 2 (Supplementary Data)

that the Val–Orn amide bond is in another environment or conformation in the heterodimer, exposing it to CID reactions. These results also indicate that peptide bonds leading to ring opening and flanking the GS pentapeptide moieties, PVOLF (or LFPVO), are protected in the GS~Srf complex. One part of the GS molecule may be participating in interaction with Srf, while a peptide moiety containing an Orn may be exposed leading to the formation of the PVO and PV fragments (Figure 7a). Refer to Supplementary Figure 15 for examples of product ion spectra and Supplementary Table 2 for details on the product ions in the Supplementary Data.

As Srf consisted of several peptides, we focused our structural study on the most abundant variant group, namely Srf_3 with *m/z* = 1022.6752. In a 2D nuclear magnetic resonance study by Eyéghé-Bickong [55] it was found that the most abundant peptide sequence in the Srf lipopeptide complex used in this study is L-Glu-L-Leu-D-Leu-L-Val-L-Asp-D-Leu-L-Leu (ELLVDLL). From the CID product ions it was deduced that C_{14} is the major fatty acyl group in the Srf_3 variant group. We found two major peaks for Srf_3 with UPLC-MS, whereas IM-MS only showed one major peak (Figure 3a, and Supplementary Figure 11 in Supplementary Data). This indicated two major species with nearly similar CCS, but slightly different hydrophobicity. From these data we deduced the major Srf_3 variant structure as cyclo[($C_{14}H_{26}O_2$)-L-Glu-L-Leu-D-Leu-L-Val-L-Asp-L-Leu-L-X] with X as Ile or Leu. For Srf the ring opening generally occurs at the lactone bond [56]. The CID of the Srf (*m/z* = 1022.6752) led to all the major product ions from the b-series, except b_6 (C_{14}ELLVD) (Figure 7b). The absence of the b_6 fragment ion is expected as the N-terminal peptide bond of an acidic residue is very labile [57]. Internal fragments and the entire y-series of product ions were also observed in the CID spectrum of free Srf (Figure 7b). The hydroxylated y_6 ion (LLVDLX) showed the highest abundance at 17%, with most of the other product ions at 2% to 7% abundance (Figure 7b and Figure 8). As for the GS product ions, most of the Srf fragments from GS~Srf_3 was generated at similar abundances to that of free Srf_3 (Figure 7b). The most dominant product ion was also the hydroxylated y_6-fragment, but its abundance increased to 24% (Figure 7b and Figure 8). The decarboxylated y_2 ion (LL or internal fragment LX) and y_6 ion (LLVDLX) were not observed (Figure 7b and Figure 8). This indicates that the carboxyl group of LL/LX is protected in the heterodimer, whereas y_6 ion (LLVDLX) is not formed, probably because the Srf interaction with GS favors the y_6 hydroxylation reaction. These results further indicate that peptide bonds in the Srf peptide moiety, LLVDLX, and especially the highly labile N-terminal bond of the Asp residue, were protected in the GS~Srf complex. On the other hand, the peptide bonds in which Glu, the other acidic residue in Srf, participates, were not protected in GS~Srf_3 as CID generated a substantial amount of the b_2 ion (C_{14}E), indicating similar exposure in the oligomer than in the free Srf_3. If the C_{14}E is imbedded in the Srf micelles, obstructing GS interaction, this moiety will be exposed to fragmentation reactions, resulting in the b_2 ion, when the hydrophobic effect is removed during the dehydration in the mass spectrometer [23–25]. Refer to Supplementary Figure 15 for examples of product ion spectra and Supplementary Table 2 for details on the product ions of Srf_3 and GS~Srf_3 heterodimer in Supplementary Data.

Conclusions

Our results corroborate the hypothesis that the cationic GS and anionic Srf interact to form GS~Srf hetero-oligomers. These noncovalent interactions could be a factor in the observed antagonism of the GS antimicrobial activity by Srf [1]. ESI-MS of the equimolar GS:Srf mixture revealed the presence of noncovalent GS~Srf heterodimers, which were not observed in the equimolar mixture of diacetylated GS and Srf. This indicated that one or both the cationic δ-amino groups of GS are probably essential for formation of ESI-MS stable and visible GS~Srf hetero-oligomers. This study revealed that polar interactions, including ionic interactions between the two peptides could take place via a slow equilibrium pointing to an assembly process. These interactions could be shielded as stable GS~Srf hetero-oligomers were observed even in a high salt (NaCl and $CaCl_2$) environment. The CID product ions of GS~Srf_3 indicated that VOLFP (or LFPVO) from GS was not generated, whereas the hydroxylated LLVDLX fragment from Srf was the most abundant. These two sequences contain an Orn and Asp residue that can partake in an ionic and/or polar interaction(s). The flanking hydrophobic residues can partake in hydrophobic interactions that would stabilize the complex and shield such electrostatic interactions in an aqueous environment. Eyéghé-

Bickong [55] found that Srf interaction with GS places the Phe and Orn residues in a more shielded environment, indicating a role of these residues in the Srf interaction. However, from our studies, the Glu residue and the fatty acid moiety in Srf do not seem to partake in the oligomerization. This could be a strong indication that the $C_{14}E$ moiety is obscured in the Srf micellular structure [43, 47] in an aqueous environment with the Asp and flanking hydrophobic amino acids being available to interact with the VOLFP moiety in GS leading to the formation of inactive GS~Srf hetero-oligomers. Furthermore, the GS~Srf heterodimers containing the most hydrophobic Srf_3 and Srf_4 variants were the most abundant species that survived within the ESI-MS and especially during IM-MS analysis. This indicates that these heterodimers were not only the most abundant in an aqueous solution but that their hydrophobicity and possibly their micellular structures may be important in seeding interaction with GS. The IM-MS studies also indicated that Srf could have a preference for specific GS conformers, possibly those in which an optimal interaction can take place. Nearly symmetrical IM-MS peaks of the GS~Srf heterodimers further indicated a compact dimer conformation, which is dependent on specific noncovalent interactions between the two peptides.

It would be expected that K_d values for $GS{\sim}Srf \leftrightarrow GS + Srf$ would be in the low micromolar range, considering the 2- to 3-fold increase in the [GS], for example from 2 μM alone to 5 μM with the presence of Srf, which is needed to inhibit 50% *Bacillus subtilis* (bacterial) growth [1]. The deduced K_d^{app} values of 6 μM in gas phase and 1 μM in aqueous phase for $GS{\sim}Srf \leftrightarrow GS + Srf$ fell indeed within the peptides' biological concentration range. However, such antagonistic peptide–peptide interaction may not be limited to this antimicrobial peptide pair. In light of the role of such an interaction in bacterial resistance, it may be worth investigating other possible antagonistic interactions between peptides produced by cohabiting microorganisms, for example, small cyclic lipopeptides like surfactin, iturins, and fengycins, and peptides that contain the gramicidin S VOLFP sequence such as the graticins, tyrocidines, and streptocidins.

Acknowledgments

The authors thank the staff of the LCMS Central Analytical facility at the University of Stellenbosch for technical assistance with the mass spectrometry on the Synapt G2 instrument. The authors also acknowledge the two excellent reviewers who helped us to improve this paper. The project was funded by the BIOPEP Peptide Fund; M.R. thanks all the members from the BIOPEP Peptide Group who over the last two decades put in many extra hours to work on contracts in order to fund orphan research projects such as this reported study.

References

1. Rautenbach, M., Eyéghé-Bickong, H.A., Vlok, N.M., Stander, M., De Beer, A.: Direct surfactin-gramicidin S antagonism supports detoxification in mixed producer cultures of *Bacillus subtilis* and *Aneurinibacillus migulanus*. Microbiolgy **158**, 3072–3082 (2012)
2. Consden, R., Gordon, A.H., Martin, A.J.P., Synge, R.L.M.: Gramicidin S: The sequence of the amino-acid residues. Biochem. J. **41**, 596–602 (1947)
3. Rackrovsky, S., Scheraga, H.A.: Intermolecular anti-parallel β-sheet: comparison of predicted and observed conformations of gramicidin S. Proc. Natl. Acad. Sci. **77**, 6965–6967 (1980)
4. Abraham, T., Prenner, E.J., Lewis, R.N.A.H., Mant, C.T., Keller, S., Hodges, R.S., McElhaney, R.N.: Structure–activity relationships of the antimicrobial peptide gramicidin S and its analogs: aqueous solubility, self-association, conformation, antimicrobial activity, and interaction with model lipid membranes. Biochim. Biophys. Acta Biomembr. **1838**, 1420–1429 (2014)
5. Kakinuma, A., Ouchida, A., Shima, T., Sugino, H., Isono, M., Tamura, G., Arima, K.: Confirmation of the structure of surfactin by mass spectrometry. Agric. Biol. Chern. **33**, 1669–1671 (1969)
6. Kakinuma, A., Hori, M., Sugino, H., Yoshida, I., Isono, M., Tamura, G., Arima, K.: Determination of the location of lactone ring in surfactin. Agric. Biol. Chem. **33**, 1523–1524 (1969)
7. Bonmatin, J.M., Genest, M., Labbe, H., Ptak, M.: Solution three dimensional structure of surfactin: a cyclic lipopeptide studies by ^{1}H-NMR, distance geometry, molecular dynamics. Biopolymers **34**, 975–986 (1994)
8. Tsan, P., Volpon, L., Besson, F., Lancelin, J.M.: Structure and dynamics of surfactin studied by NMR in micellar media. J. Am. Chem. Soc. **129**, 1968–1977 (2007)
9. Kowall, M., Vater, J., Kluge, B., Stein, T., Franke, P., Ziessow, D.: Separation and characterization of surfactin isoforms produced by *Bacillus subtilis* OKB 105. J. Colloid Interface Sci. **204**, 1–11 (1998)
10. Bonmatin, J.M., Genest, M., Labbé, H., Grangemard, I., Peypoux, F., Maget-Dana, R., Ptak, M., Michel, M.: Production, isolation and characterization of [Leu^4]- and [Ile^4]surfactins from *Bacillus subtilis*. Lett. Pept. Sci. **2**, 41–47 (1995)
11. Baumgart, F., Kluge, B., Ullrich, C., Vater, J., Ziessow, D.: Identification of amino acid substitutions in the lipopeptide surfactin using 2D NMR spectroscopy. Biochem. Biophys. Res. Commun. **177**, 998–1005 (1991)
12. Mihailescou, D., Smith, J.C.: Atomic detail peptide–membrane interactions: molecular dynamics simulation of gramicidin S in a DMPC bilayer. Biophys. J. **79**, 1718–1730 (2000)
13. Maget-Dana, R., Ptak, M.: Interaction of surfactin with membrane models. Biophys. J. **68**, 1937–1943 (1998)
14. Pramanik, B.N., Bartner, P.L., Mirza, U.A., Liu, Y.-H., Ganguly, A.K.: Electrospray ionization mass spectrometry for the study of noncovalent complexes: an emerging technology. J. Mass Spectrom. **33**, 911–920 (1998)
15. Hilton, G.R., Benesch, J.L.P.: Two decades of studying non-covalent biomolecular assemblies by means of electrospray ionization mass spectrometry. J. R. Soc. Interface **9**, 801–816 (2012)
16. Woods, A.S., Huestis, M.A.: A study of peptide-peptide interaction by matrix-assisted laser desorption/ionization. J. Am. Soc. Mass Spectrom. **12**, 88–96 (2001)
17. Woods, A.S., Koomen, J.M., Ruotolo, B.T., Gillig, K.J., Russel, D.H., Fuhrer, K., Gonin, M., Egan, T.F., Schultz, J.A.: A study of peptide-peptide interactions using MALDI ion mobility o-TOF and ESI mass spectrometry. J. Am. Soc. Mass Spectrom. **13**, 166–169 (2002)
18. Alves, S., Woods, A., Delvolvé, A., Tabet, J.C.: Influence of salt bridge interactions on the gas-phase stability of DNA/peptide complexes. Int. J. Mass Spectrom. **278**, 122–128 (2008)
19. Haselmann, K.F., Jørgensen, T.J.D., Budnik, B.A., Jensen, F., Zubarev, R.A.: Electron capture dissociation of weakly bound polypeptide polycationic complexes. Rapid Commun. Mass Spectrom. **16**, 2260–2265 (2002)
20. Mathur, S., Badertscher, M., Scott, M., Zenobi, R.: Critical evaluation of mass spectrometric measurement of dissociation constants: accuracy and cross-validation against surface plasmon resonance and circular dichroism for the calmodulin–melittin system. Phys. Chem. Chem. Phys. **9**, 6187–6198 (2007)
21. Jørgensen, T.J.D., Delforge, D., Remacle, J., Bojesen, G., Roepstorff, P.: Collision-induced dissociation of noncovalent complexes between vancomycin antibiotics and peptide ligand stereoisomers: evidence for molecular recognition in the gas phase. Int. J. Mass Spectrom. **188**, 63–85 (1999)

22. Penn, S.G., He, F., Green, M.K., Lebrilla, C.B.: The use of heated capillary dissociation and collision-induced dissociation to determine the strength of noncovalent bonding interactions in gas-phase peptide–cyclodextrin complexes. J. Am. Soc. Mass Spectrom. **8**, 244–252 (1997)
23. Cubrilovic, D., Biela, A., Sielaff, F., Steinmetzer, T., Klebe, G., Zenobi, R.: Quantifying protein-ligand binding constants using electrospray ionization mass spectrometry: a systematic binding affinity study of a series of hydrophobically modified trypsin inhibitors. J. Am. Soc. Mass Spectrom. **23**, 1768–1777 (2012)
24. Bich, C., Baer, S., Jecklin, M.C., Zenobi, R.: Probing the hydrophobic effect of noncovalent complexes by mass spectrometry. J. Am. Soc. Mass Spectrom. **21**, 286–289 (2010)
25. Wu, Q., Gao, J., Joseph-Mccarthy, D., Sigal, G.B., Bruce, J.E., Whitesides, G.M., Smith, R.D.: Carbonic anhydrase-inhibitor binding: from solution to the gas phase. J. Am. Chem. Soc. **119**, 1157–1158 (1997)
26. Daniel, J.M., Friess, S.D., Rajagopalan, S., Wendt, S., Zenobi, R.: Quantitative determination of noncovalent binding interactions using soft ionization mass spectrometry. Int. J. Mass Spectrom. **216**, 1–27 (2002)
27. Rautenbach, M., Swart, P., Van Der Merwe, M.J.: Sequence specific stabilization of a linear analogue of iturin A_2 with sodium under low energy ESI-MS conditions. J. Am. Soc. Mass Spectrom. **12**, 505–516 (2001)
28. Wysocki, V.H., Tsaprailis, G., Smith, L.L., Breci, L.A.: Mobile and localized protons: A framework for understanding peptide dissociation. J. Mass Spectrom. **35**, 1399–1406 (2000)
29. Mann, M., Steen, H.: The ABC's (and XYZ's) of peptide sequencing. Nat. Rev. Mol. Cell Biol. **5**, 699–711 (2004)
30. Ruotolo, B.T., Benesch, J.L.P., Sandercock, A.M., Hyung, S.-J., Robinson, C.V.: Ion mobility-mass spectrometry analysis of large protein complexes. Nat. Protoc. **3**, 1139–1152 (2008)
31. Bush, M.F., Campuzano, I.D., Robinson, C.V.: Ion mobility mass spectrometry of peptide ions: effects of drift gas and calibration strategies. Anal. Chem. **84**, 7124–7130 (2012)
32. Douglas, D.J.: Applications of collision dynamics in quadrupole mass spectrometry. J. Am. Soc. Mass Spectrom. **9**, 101–113 (1998)
33. Mayer, P.M., Martineau, E.: Gas-phase binding energies for noncovalent Ab-40 peptide/small molecule complexes from CID mass spectrometry and RRKM theory. Phys. Chem. Chem. Phys. **13**, 5178–5186 (2011)
34. Gabelica, V., Galic, N., Rosu, F., Houssier, C., De Pauw, E.: Influence of response factors on determining equilibrium association constants of noncovalent complexes by electrospray ionization mass spectrometry. J. Mass Spectrom. **38**, 491–501 (2003)
35. Liu, J., Konermann, L.: Protein–protein binding affinities in solution determined by electrospray mass spectrometry. J. Am. Soc. Mass Spectrom. **22**, 408–417 (2011)
36. Chao, H., Houston Jr., M.E., Grothe, S., Kay, C.M., O'Connor-McCourt, M., Irvin, R.T., Hodges, R.S.: Kinetic study on the formation of a de novo designed heterodimeric coiled-coil: use of surface plasmon resonance to monitor the association and dissociation of polypeptide chains. Biochemistry **35**, 12175–12185 (1996)
37. Ruotolo, B.T., Tate, C.C., Russell, D.H.: Ion mobility-mass spectrometry applied to cyclic peptide analysis: conformational preferences of gramicidin S and linear analogs in the gas phase. J. Am. Soc. Mass Spectrom. **15**, 870–878 (2004)
38. Goodwin, C.R., Fenn, L.S., Derewacz, D.K., Bachmann, B.O., McLean, J.A.: Structural mass spectrometry: rapid methods for separation and analysis of peptide natural products. J. Nat. Prod. **75**, 48–53 (2012)
39. Shukla, A.K., Futell, J.H.J.: Tandem mass spectrometry: dissociation of ions by collisional activation. J. Mass Spectrom. **36**, 1069–1090 (2000)
40. Danders, W., Marahiel, A.M., Krause, M.I., Kosui, N., Kato, T., Izumiya, N., Kleinkauf, H.: Antibacterial action of gramicidin S and tyrocidines in relation to active transport, in vitro transcription, spore outgrowth. Antimicrob. Agents Chemother. **22**, 785–790 (1982)
41. Nagamurthi, G., Rambhav, S.: Gramicidin S: structure–activity Relationship. J. Biosci. **7**, 323–329 (1985)
42. Thimon, L., Peypoux, F., Wallach, J., Michel, G.: Ionophorous and sequestering properties of surfactin, a biosurfactant from *Bacillus subtilis*. Colloids Surf. B **1**, 57–62 (1993)
43. Osman, M., Høiland, H., Holmsen, H., Ishigami, Y.: Tuning micelles of a bioactive heptapeptide biosurfactant via extrinsically induced conformational transition of surfactin assembly. J. Pept. Sci. **4**, 449–458 (1998)
44. Vass, E., Besson, F., Majer, Z., Volpon, L., Hollosi, M.: Ca^{2+}-induced changes of surfactin conformation: a FTIR and circular dichroism Study. Biochem. Biophys. Res. Commun. **282**, 361–367 (2001)
45. Sheppard, J.D., Jumarie, C., Cooper, D.G., Laprade, R.: Ionic channels induced by surfactin in planar lipid bilayer membranes. Biochim. Biophys. Acta **1064**, 13–23 (1991)
46. Heerklotz, H., Seelig, J.: Detergent-like action of the antibiotic peptide surfactin on lipid membranes. Biophys. J. **81**, 1547–1554 (2001)
47. Ishigami, Y., Osman, M., Nakahara, H., Sano, Y., Ishiguro, R., Matsumoto, M.: Significance of β-sheet formation for micellization and surface adsorption of surfactin. Colloids Surf B **4**, 341–348 (1995)
48. Rautenbach, M., Swart, P., Van Der Merwe, M.J.: The interaction of analogues of the antimicrobial lipopeptide, iturin A_2, with alkali metal ions. Bioorg. Med. Chem. **8**, 2539–2548 (2000)
49. Thibault, P., Faubert, D., Karunanithy, S., Boyd, R.K., Holmes, C.F.: Isolation, mass spectrometric characterization, protein phosphatase inhibition properties of cyclic peptide analogues of gramicidin-S from *Bacillus brevis* (Nagano strain). Biol. Mass Spectrom. **21**, 367–379 (1992)
50. Pittenauer, E., Zehl, M., Belgacem, O., Raptakis, E., Mistrik, R., Allmaier, G.: Comparison of CID spectra of singly charged polypeptide antibiotic precursor ions obtained by positive-ion vacuum MALDI IT/RTOF and TOF/RTOF AP-MALDI-IT and ESI-IT mass spectrometry. J. Mass Spectrom. **4**, 421–447 (2006)
51. Schwartz, B.L., Bursey, M.M.: Some proline substituent effects in the tandem mass spectrum of protonated pentaalanine. Biol. Mass Spectrom. **21**, 92–96 (1992)
52. Raulfs, M.D.M., Breci, L., Bernier, M., Hamdy, O.M., Janiga, A., Wysocki, V., Poutsma, J.C.: Investigations of the mechanism of the "proline effect" in tandem mass spectrometry experiments: the "pipecolic acid effect". J. Am. Soc. Mass Spectrom. **25**, 1705–1715 (2014)
53. Mcgee, W.M., Mcluckey, S.A.: The ornithine effect in peptide cation dissociation. J. Mass Spectrom. **48**, 856–861 (2013)
54. Crittinden, C.M., Parker, W.R., Jenner, Z.B., Bruns, K.A., Akin, L.D., Mcgee, W.M., Ciccimaro, E., Brodbelt, J.S.: Exploitation of the ornithine effect enhances characterization of stapled and cyclic peptides. J. Am. Soc. Mass Spectrom. **27**, 856–863 (2016)
55. Eyéghé-Bickong, H.A.: Role of surfactin from *Bacillus subtilis* in protection against antimicrobial peptides produced by selected *Bacillus* species. Ph.D. thesis, Stellenbosch University. http://scholar. sun.ac.za/ handle/10019.1/6773, pp. 3.26–3.38 (2011).
56. Hue, N., Serani, L., Lapre'Vote, O.: Structural investigation of cyclic peptidolipids from *Bacillus subtilis* by high-energy tandem mass spectrometry. Rapid Commun. Mass Spectrom. **15**, 203–209 (2001)
57. Gu, C., Tsaprailis, G., Breci, L., Wysocki, V.H.: Selective gas-phase cleavage at the peptide bond C-terminal to aspartic acid in fixed-charge derivatives of Asp-containing peptides. Anal. Chem. **72**, 5804–5813 (2000)